ACS APPLIED ENERGY MATERIALS

www.acsaem.org Article

Band Tails and Cu−Zn Disorder in Cu_2ZnSnS_4 Solar Cells

J. K. Larsen,* J. J. S. Scragg, N. Ross, and C. Platzer-Björkman

Cite This: *ACS Appl. Energy Mater.* 2020, 3, 7520−7526 Read Online

ACCESS | Metrics & More | Article Recommendations | Supporting Information

ABSTRACT: Cu_2ZnSnS_4 (CZTS) has attracted interest for applications in thin-film solar cells. In this study, the annealing process for CZTS fabrication is systematically varied, resulting in a large variation of materials properties. These variations are connected to the sulfur partial pressure during the annealing. A well-known phenomenon in CZTS is the presence of a high density of Cu−Zn antisite defect pairs, also known as Cu−Zn disorder. Faster Cu−Zn ordering occurs in samples with a similar starting composition annealed in an atmosphere with a higher sulfur partial pressure. This is explained by a higher density of vacancies in these samples. The results indicate that reduction of the vacancy concentration in CZTS annealed in insufficient sulfur partial pressure reduces diffusion, which results in more defective material with a higher density of tail states and poorer device performance.

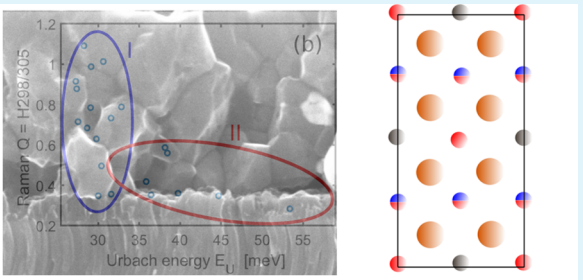

KEYWORDS: *kesterite, CZTS, thin-film photovoltaics, band tails, disorder, voltage deficit*

1. INTRODUCTION

$Cu_2ZnSnS(e)_4$ [CZTS(e)] has been studied extensively in recent years since it is considered a promising alternative to the more established material $Cu(In,Ga)Se_2$ (CIGS) for application in thin-film solar cells. The advantage of CZTS over CIGS is that less abundant indium is replaced with more earth-abundant zinc and tin. CZTS devices are often highlighted for the use of only nontoxic elements, even though Cd is typically used in the CdS buffer layer. The highest efficiency obtained to date for CZTS with a CdS buffer layer is 11%,[1] while the highest efficiency obtained for a Cd-free CZTS device is 10.2%.[2] In spite of the progress in the understanding of CZTS, it remains challenging to produce CZTS with sufficiently good properties to reach efficiency levels demonstrated with the CIGS technology (23.35%[3]). Issues that have been suggested to contribute to the limited efficiency of CZTS solar cells include band tails,[4,5] Cu−Zn disorder,[6] deep defects,[7] interface recombination,[1,8] and multiphase films.[9] In this study, we focus on the relationship between annealing conditions and the resulting Cu−Zn disorder and band tails.

Due to the similarity of Cu^+ and Zn^{2+}, $\{Cu_{Zn}^- + Zn_{Cu}^+\}^0$ antisite defect pairs are abundant in CZTS.[10] The high concentration of Cu−Zn antisite defect complexes is often called Cu−Zn disorder because its formation can be described by a second-order phase transition with a critical temperature T_c. Above T_c, the CZTS is completely "disordered" and Cu and Zn are randomly distributed on the 2c and 2d lattice positions. At temperatures below the critical temperature, the Cu and Zn atoms will partially reorganize to their correct lattice sites. Slow cooling of the material can therefore reduce the density of Cu−Zn defect complexes, and "more ordered" CZTS can be obtained.[6,11] The phenomenon has been studied in detail for CZTS,[6,11,12] CZTSe,[13] and CZTSSe alloys.[14] The cooling rate is important when comparing CZTS materials since the degree of relative disorder is determined during the cooling stage.[12] Since the ordering process is assisted by the presence of vacancies, the final ordering in the CZTS material is sensitive to the type of defect complexes in the material, i.e., to the type of off-stoichiometry of the CZTS phase.[15−17]

Typically, tail states in semiconductors are ascribed to "disorder" resulting in broken symmetries that split degenerate states toward lower and higher energies.[18] The term disorder used in this context is somewhat vague, and can include multiple physical phenomena, including a high concentration of defect complexes, as well as crystalline imperfections (e.g., dislocations and stacking faults) and compositional inhomogeneities. The result of these imperfections is a rapidly decaying density of states extending into the band gap. In recent studies, it is argued that the band tails in CZTSe are not dominated by Cu−Zn disorder.[4,19] This conclusion was reached after a study of the band tails by photoluminescence (PL) before and after ordering treatments. Instead, it is argued that tail states are caused by a combination of band gap fluctuations caused by chemical composition variations at the nanoscale and electrostatic potential fluctuations caused by a

Received: April 22, 2020
Accepted: July 20, 2020
Published: July 20, 2020

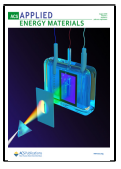

https://dx.doi.org/10.1021/acsaem.0c00926
ACS Appl. Energy Mater. 2020, 3, 7520−7526

Table 1. Composition of Precursors Measured by XRF, and Annealing Parameters Used for Each Sample Series

series	Cu/Sn	Zn/(Cu + Sn)	Sn/(Cu + 2Zn)	time (min)	Ar pressure (mbar)	S dose (g)
time	1.91	0.36	0.25	1, 3, 5, 10, 15, 20	350	3
pressure I	1.93	0.35	0.26	10	1, 50, 100, 250, 900	3
pressure II	1.89	0.37	0.25	10	200, 350, 500, 650, 800	3
sulfur dose	1.85	0.37	0.25	10	500	0, 1, 2, 3

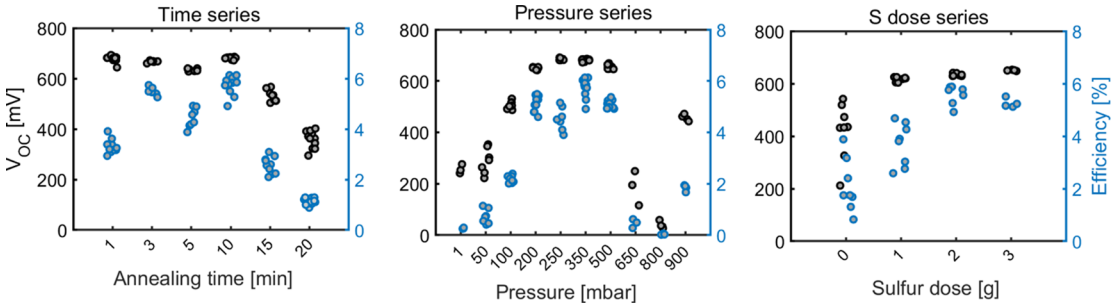

Figure 1. V_{oc} and efficiency of devices fabricated with various sulfurization process conditions.

high concentration of compensated defects.[4] Multiple reports suggest that band tails are one of the limiting mechanisms in CZTS(e).[4,5,20−22] It is argued that the band tails contribute to charge carrier recombination,[22] thereby introducing a large nonradiative voltage loss that limits the open-circuit voltage (V_{oc}) of the solar cell.

Our approach to synthesis of CZTS involves sputtering of Cu−Zn−Sn−S precursors from binary targets followed by annealing in a sulfur-containing atmosphere, also called sulfurization. When using this approach, the absorber properties are significantly affected by the parameters of the sulfurization process. It is well established that the sulfur partial pressure during annealing of CZTS is critically important.[23,24] In the absence of sufficient sulfur in the annealing atmosphere, the surface of CZTS decomposes, and in the worst case, SnS evaporates, rendering the decomposition irreversible.[23] This has been shown to have a strong impact on the device performance, as the V_{oc} values of devices were improved when sufficient sulfur was supplied.[24] This approach was recently applied to reach a V_{oc} of 809 mV for a CZTS device.[25]

In this study, the parameter space of the annealing process is investigated, with a view to probing the dependence of V_{oc} (and related material properties) on sulfur pressure in more detail. As a result, CZTS samples with widely different properties are produced. The relationship between V_{oc} deficit, band tails, and Cu−Zn disorder is investigated by a combination of photoluminescence, quantum efficiency (QE), and Raman spectroscopy. The observations are related to annealing conditions in an attempt to better understand the possible origin of band tails and voltage deficit in CZTS with device-relevant Cu-poor and Zn-rich composition.

2. METHODS

Absorbers were prepared by deposition of precursors followed by annealing in a sulfur-containing graphite reactor. Precursors were sputtered from CuS, SnS, and ZnS binary targets on Mo-coated glass substrates at 250 °C. The compositions of the precursors, measured by X-ray fluorescence (XRF), are shown in Table 1. Following the notation introduced by Lafond et al., the precursors are expected to be of A-type.[26]

Precursors were annealed in a furnace within a 3 L graphite reactor with a separately heated source used to dose controlled quantities of sulfur into the reactor. The annealing system is different from the tube furnace used in previous publications by the group, e.g., ref 24. More details regarding the custom-built system used in this work is available in ref 27. The reactor is preheated to a set temperature of 560 °C before the sample—resting in a graphite carrier—is introduced. Immediately after sample introduction, sulfur is dosed into the preheated source at 560 °C and brought into the reactor with a flow of argon carrier gas in the course of 1 min. The reactor is then sealed for an annealing dwell step. In this work, the argon background pressure, annealing time, and sulfur dose were varied in three different experimental series. In the time series, the pressure was 350 mbar, and sulfur dose was 3 g, while the time was varied from 1 to 20 min. In the pressure series, the time was 10 min, the sulfur dose was 3 g, while the pressure was varied from 1 to 900 mbar. One set of precursors were used for pressure series I. These were annealed with Ar pressures of 1, 50, 100, 250, and 900 mbar. Precursors with a slightly different composition used for pressure series II were annealed at 200, 350, 500, 650, and 800 mbar. Finally, in the sulfur dose series, time was 10 min, pressure was 500 mbar, while the sulfur dose was varied from 0 to 3 g. The samples were allowed to cool naturally within the reactor for an hour, after which the temperature is about 90 °C. Samples are then transferred to a load lock and rapidly cooled to room temperature. All samples studied here experienced the same cooling rate.

Raman measurements were performed on the absorber material (not completed devices) in a Renishaw inVia using 785 nm laser excitation. Fitting of the spectra is performed using 11 Lorentzian peaks. Photoluminescence measurements have been performed in the same system, utilizing a 532 nm laser for excitation. To determine the peak positions, the spectra are corrected for interference effects using the approach described in ref 28. The composition of precursors was measured by XRF. The composition of the annealed samples was measured by energy-dispersive X-ray spectroscopy (EDS) with an acceleration voltage of 10 kV, calibrated with XRF.

To prepare devices, the absorbers were etched for 2 min in 5% KCN immediately before CdS deposition. CdS was deposited by chemical bath deposition following the procedure described in ref 29. The preparation of the devices was completed by sputter deposition of an intrinsic ZnO (i-ZnO)/Al:ZnO bilayer and mechanical scribing to define cells with an area of 0.05 cm^2. *JV* measurements were performed using a Newport ABA solar simulator, and quantum efficiency measurements were performed in a homebuilt setup. The optical reflectance of the samples was measured with a Bentham PVE300 system to calculate the internal quantum efficiency. The internal quantum efficiency is calculated as IQE = EQE/(1 − *R*), where EQE is the external quantum efficiency and *R* is the reflectance.

https://dx.doi.org/10.1021/acsaem.0c00926
ACS Appl. Energy Mater. 2020, 3, 7520−7526

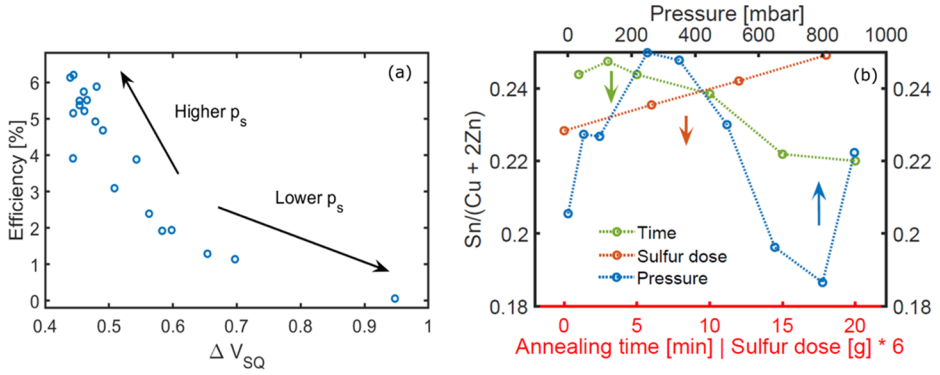

Figure 2. (a) Correlation between voltage deficit and efficiency. (b) Compositional ratio Sn/(Cu + 2Zn) of the absorber measured by EDS after annealing for various annealing conditions. Note that the annealing time and sulfur dosing share the bottom *x*-axis, but the sulfur dose is scaled by a factor of 6.

All of the measurement data, on which the analysis in this paper is based, can be found in the Supporting Information (SI).

3. RESULTS AND DISCUSSION

3.1. Device Performance and Sulfur Loss. The measured open-circuit voltage, V_{oc}, and efficiency of the devices prepared in the three experimental series are shown in Figure 1. The annealing time has a minor effect on V_{oc} until 10 min of dwell time. For longer anneals, V_{oc} and efficiency are reduced. A plausible explanation for the reduction of V_{oc} and efficiency for longer anneals is loss of sulfur from the reaction zone. This effect has previously been demonstrated, using the decomposition reaction of SnS_2 monitor samples to track sulfur loss from the reactor.[24]

The pressure series in Figure 1 shows a plateau in the range of 200−500 mbar. When either a higher or lower background pressure is used, both V_{oc} and efficiency are reduced. The poor performance when using a low background pressure can be explained by faster loss of sulfur from the immediate surroundings of the sample. The decrease in efficiency for the highest Ar background pressure could likewise be related to a lower sulfur pressure; since the sulfur is brought into the reactor with a carrier gas, the presence of a high Ar pressure in the reactor can hinder efficient transport of the sulfur vapor to the sample position. In the final series, where the sulfur dose is varied, it is observed that a lower dose of sulfur results in poorer devices. It should be noted that in these experiments, a small background partial pressure of S_2 and SnS_x are expected in the reactor due to residues from previous runs. A dose of 0 g of sulfur does therefore not imply that no sulfur was present in the atmosphere. To monitor compositional changes, EDS measurement of the absorber composition after annealing was performed, as shown in Figure 2b. It is well known that annealing of CZTS in an atmosphere containing insufficient sulfur results in loss of Sn from the sample.[30] In the present sample series, a Sn loss is observed in the samples with poorer performance, as seen in Figure 2b.

As a measure of voltage deficit, the ratio between the measured device V_{oc} and the open-circuit voltage in the Shockley−Queisser limit, $V_{oc,SQ}$, is used: $\Delta V_{SQ} = 1 - \frac{V_{OC}}{V_{OC,SQ}}$. The maximum attainable $V_{oc,SQ}$ for a given band gap is based on ref 31. Band gaps extracted from fitting of the IQE spectrum form the basis for the determination of $V_{oc,SQ}$ for each device (more details on band gap extraction are given in the SI). $V_{oc,SQ}$ for the highest-band-gap and lowest-band-gap samples are 1.12 and 1.25 V, respectively. Figure 2a shows the voltage deficit ΔV_{SQ} of the best device from each sample in all of the three series. It is clearly noted that the poor devices are characterized by a larger voltage deficit, while the better devices have a lower voltage deficit. Even the best devices are, however, significantly limited by a voltage deficit of ΔV_{SQ} = 0.45.

3.2. Band Tails. Two models are compared to characterize the band tails in the studied CZTS devices. Both approaches rely on fitting of the absorption edge of the IQE spectra. Details regarding the models as well as fit examples can be found in the SI. One model assumes that an exponentially decaying absorption coefficient can be described by a characteristic Urbach energy (E_U) below the optical band gap.[32] The Urbach energy determined from fitting the IQE is shown in Figure 3. The other model applied in this work

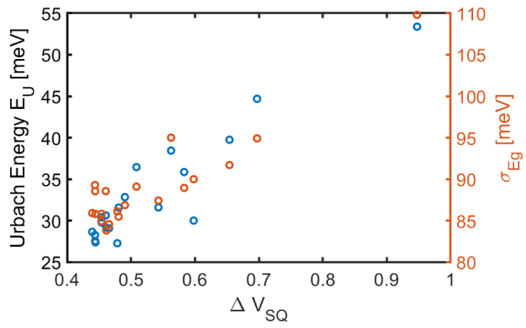

Figure 3. (Left axis) Correlation between Urbach energy E_U and voltage deficit. (Right axis) Correlation between the standard deviation σ_{E_g} of the Gaussian band gap distribution and voltage deficit.

assumes that the absorption edge can be better described with a Gaussian distribution of band gaps centered around an average band gap $E_{g,mean}$, with a standard deviation σ_{E_g}. A similar approach has been applied to describe the band tails of CZTS in a few studies.[4,5,32] The standard deviations of the band gap distributions obtained by fitting are shown in Figure 3.

It is found that both models applied to fit the band tails yield similar results when comparing extracted tail states extension and V_{oc} deficit. An increase of the extension of tail states is observed with increasing V_{oc} deficit. This is in agreement with the empirical relationship between V_{oc} deficit and Urbach energy of various PV materials presented by de Wolf et al.[33] A

https://dx.doi.org/10.1021/acsaem.0c00926
ACS Appl. Energy Mater. 2020, 3, 7520−7526

similar trend was presented by Miller et al. for CZTSSe devices with various S/(S + Se) concentrations.[34] In that case, higher V_{oc} deficit and E_U values are found in devices with higher S/(S + Se) ratios. These findings all support the idea that materials with a high E_U, i.e., a higher density of band tail states, suffer from more severe V_{oc} losses.

It is worth noting that the IQE measurement only gives information on the charge carriers in tail states that are collected. Deeper band tails can exist that do not allow for charge transport and collection. These still affect the V_{oc} deficit without showing up in IQE measurements. Information regarding deeper tail states might be accessible with photoluminescence.[35] As seen in Figure 4b, the PL peak is up to 200

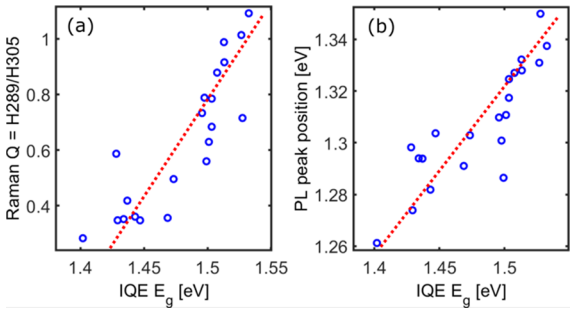

Figure 4. (a) Correlation between order parameter and band gap determined from IQE. (b) Correlation between PL peak position and band gap energy.

meV lower than the IQE band gap. An example of excitation-dependent PL intensity is shown in Figure S7 in the SI. The relationship between luminescence intensity (I_{PL}) and excitation density (P_{ext}) follows the power law: $I_{PL} \propto P_{ext}^{k}$. Here, we find k = 1.39, which could indicate that the PL peak relates to band-tail-to-band-tail (TT) recombination,[35] demonstrating radiative recombination via deep tail states. However, it cannot be ruled out that the transition could relate to free-to-bound (FB) recombination involving the acceptor state recombination[36] (see discussion in the SI for further details).

It has been suggested that tail states play an important role in recombination in CZTSe.[22] The correlation found here is not proof that this is the case, but it supports the hypothesis that tail states could be a part of the explanation for the large V_{oc} deficit in CZTS. The Shockley–Read–Hall (SRH) recombination via tail states has likewise been identified as playing a role in other materials such as heavily doped Si[37] and organic semiconductors.[38]

3.3. Variation in Cu–Zn Order. Raman spectroscopy is sensitive to defects in materials.[39,40] In particular, it has been demonstrated that the Raman spectrum of CZTS is significantly affected by Cu–Zn disorder.[11] As a measure of the relative Cu–Zn disorder, we use the ratio of the Raman modes at 289 and 305 cm^{-1}: Q = H289/H305.[11] These were extracted by fitting the Raman spectra with 11 peaks after removal of the background. It is well known that increased Cu–Zn order, as measured here by the Q parameter, increases the optical band gap. This has been studied for CZTS,[6,11] CZTSe,[13] and CZTSSe alloys.[14]

Figure 4a shows the relationship between the order parameter and the band gap determined from IQE by fitting of the band edge with a Gaussian distribution of band gaps. The linear Pearson correlation coefficient of the data is 0.85, demonstrating a strong correlation. As mentioned, one has to be aware of the influence of charge carrier collection on the band edge extracted from IQE.[32] This is especially true in poorly performing devices where the collection efficiency can severely affect the shape of the absorption onset measured by QE. To ensure that the variation in band gap is truly related to the effect of ordering rather than an artifact of the band gap extraction, PL measurements on the same samples are presented in Figure 4b. After correction of the interference effects in the PL spectra following the approach presented previously,[28] the PL peak maxima were determined. The linear Pearson correlation coefficient of the PL vs IQE E_g data is 0.87, again demonstrating a strong correlation. The blue shift of both the PL peak and band gap with increased ordering confirms that the band gap extracted from QE is not solely an artifact of variation of collection efficiency.

The fact that some absorbers end up with a lower degree of order, given that the thermal history is the same for all samples, is thought to be related to the interplay between the conditions of the thermal process and the composition of the CZTS phase explored by Davydova et al. in ref 15. In that paper, it was proposed that the concentrations of the various types of neutral defect complexes (named A- to J-type) in CZTS are dependent on the sulfur and SnS partial pressures during annealing. In particular, neutral defect complexes containing vacancies or interstitials have a strong positive effect on the rate of diffusion and cation ordering.[16]

There are two relevant complexes for the CZTS compositions used here: (1) "A-type", consisting of Cu vacancies paired with a Zn on Cu antisites, i.e., $\{V_{Cu}^{-} + Zn_{Cu}^{+}\}^{0}$, and giving Cu-poor, Zn-rich composition; (2) "B-type", formed by introduction of positively charged Zn on Cu antisites in combination with a negatively charged Zn on Sn antisites, i.e., $\{2Zn_{Cu}^{+} + Zn_{Sn}^{2-}\}^{0}$, and giving purely Zn-rich CZTS.

Based on the composition of the precursors measured by XRF, they are expected to be close to stoichiometric and contain primarily A-type defects. When annealing the A-type CZTS in an atmosphere with insufficient sulfur and SnS partial pressures, A-type defects can be turned into B-type defects via loss of S and SnS, as proposed in ref 15

$$2\{V_{Cu}^{-} + Zn_{Cu}^{+}\}^{0} \rightleftharpoons \{2Zn_{Cu}^{+} + Zn_{Sn}^{2-}\}^{0} + 2SnS\,(g/s) + S_2\,(g) \quad (1)$$

This reaction corresponds to the elimination of vacancies in the CZTS phase, which is expected to result in a decreasing diffusion rate and a slower rate of ordering upon subsequent cooling.[15,16] Since a shift of the equilibrium in eq 1 to the right is expected to result in a change of the sample composition, EDS measurements calibrated to the XRF were performed as shown in Figure 2b. The ratio Sn/(Cu + 2Zn) is expected to be 0.25 in A-type CZTS, while reducing when the fraction of B-type defect complexes is increased. Generally, a lower Sn/(Cu + 2Zn) ratio is observed for sulfur-deficient annealing conditions. Figure S2 shows the measured compositions of the precursors along with the annealed absorbers. The result confirms that the initially A-type CZTS precursors either remain A-type or become B-type CZTS during the annealing process. The loss of vacancies when A-type CZTS becomes B-type CZTS explains the lower degree of Cu–Zn order when annealing with insufficient sulfur. Depth profiling (Figure S3) indicates that the loss of Sn primarily affects the top part of the

https://dx.doi.org/10.1021/acsaem.0c00926
ACS Appl. Energy Mater. 2020, 3, 7520–7526

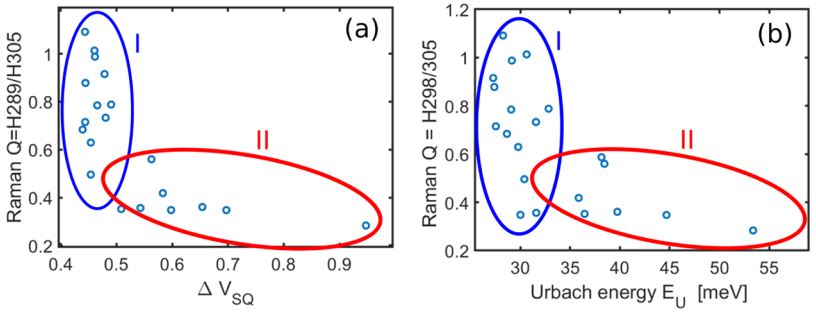

Figure 5. (a) Correlation between order parameter and voltage deficit. (b) Correlation between Urbach energy and order parameter.

film. It is therefore expected that the surface region contains a significantly larger fraction of B-type complexes than indicated by XRF. The nonuniform depth distribution could have a significant effect on the device performance since the devices will likely be dominated by properties of the surface near part of the film.

3.4. Relation between Band Tails, Cu−Zn Order, and Voltage Deficit. We have established that the set of samples contains materials with a wide range of tail state densities, Cu−Zn disorder, and voltage deficit. The differences can primarily be explained in terms of the variation of the sulfur partial pressure during annealing. It is now interesting to investigate relationships between these properties.

Figure 5a shows the correlation between the Q parameter and V_{oc} deficit. The data can be described as two groups. Group I contains devices with a lower voltage deficit and a large spread in the order parameter Q. The large spread in order within this group shows that reduced disorder does not necessarily lead to a reduced V_{oc} deficit. This finding is in agreement with several other studies,[14,20,25,35] also finding that reduction of disorder does not necessarily reduce the V_{oc} deficit. Figure 5b shows the correlation of the Q parameter and the Urbach energy. Two groups of data points can also be identified. Group I contains devices with similar Urbach energies of around 30 meV and a wide range of Q parameter values. The spread of data points inside this group indicates that a reduction of Cu−Zn disorder in itself does not necessarily reduce the Urbach energy. This finding agrees with earlier studies that conclude that Cu−Zn disorder is not the main cause of band tails in CZTS.[19,35,41] This conclusion was reached based on the analysis of the PL spectra of CZTSSe before and after thermal ordering treatments by Rey et al.[35] The study of Malerba et al. reached the same conclusion by changing the degree of order within a device by an annealing treatment and measurement of the band tails with EQE.[41] In this study, we see evidence for Cu−Zn disorder not being the primary cause of band tails based on the analysis of QE spectra in combination with Raman spectroscopy, thereby confirming earlier findings.

While group I in Figure 5a,b indicates that neither tail states nor voltage deficit is caused directly by disorder, both figures also contain group II with samples that stand out. The samples in group II are the ones annealed at either a too high or too low Ar background pressure, or for a too long time (samples with low V_{oc} in Figure 1). Under these conditions, insufficient sulfur is supplied and Sn is lost from the sample, as seen in Figure 2b. This group of samples is characterized by low V_{oc}, low degree of ordering, and large density of tail states. This is an indication that the type of defect that causes the tails (i.e., the high Urbach energies) is associated with conditions for which Cu−Zn ordering is also slow. Following earlier discussion, this implies that the defects responsible for the tail state formation are not vacancies since a high concentration of vacancies would promote fast ordering.

The finding that devices with a high density of tail states and a high voltage deficit are also characterized by a high degree of Cu−Zn disorder (group II) gives an indication of the cause. A possible explanation relates to diffusion within the material. It could be that presence of vacancies in the lattice plays an important role in reduction of detrimental defects. Vacancies generally improve diffusion and allow formation of more "perfect" material, e.g., elimination of defects of any kind, whether dislocations, stacking faults, Cu−Zn disorder, or any other metastable disorder. Having good diffusion during growth would be the key to eliminating all kinds of disorder in the material, and vacancies might be the key to this. In CZTS, it can only be ensured that a high concentration of vacancies is present if annealing is performed in the presence of a high S partial pressure. This explains the observed behavior, where poor devices with a large voltage deficit are characterized by a low degree of order as well as a high density of tail states. Material annealed in a higher sulfur partial pressure, on the other hand, suffers less from tail states possibly due to a higher vacancy concentration that allows faster diffusion and annihilation of defects. Hindered diffusion would also be expected to result in smaller grains in samples annealed in insufficient sulfur. Figure S4 shows examples of this by cross-sectional scanning electron microscopy (SEM). Samples in group II show smaller grains or less well-defined grains compared to samples in group I. A general tendency of wider X-ray diffraction peaks is also observed in samples with a larger V_{oc} deficit as seen in Figure S5. These observations indicate that poor recrystallization possibly due to loss of Sn from the surface and hindered diffusion could be the cause of poor device performance of samples in group II. It has to be kept in mind that the Sn loss was observed to primarily affect the top of the film. The degraded properties of the uppermost absorber and interface could therefore play a key role in the poor performance.

One can imagine different ways to improve diffusion during growth and therefore the properties of CZTS. Simply increasing the temperature is one approach, but it is difficult to realize due to the limitations of the substrate and decomposition of CZTS.[23] Another approach could be the use of additives or low temperature melting secondary phases that act as fluxing agents. It has been argued that liquid Cu_xSe plays this role in CIGS,[42] which explains the success of the three-stage process. Similarly, it has been demonstrated that the $CdCl_2$ treatment improves the properties of CdTe because of enhanced diffusion.[43] Identification of a suitable fluxing

https://dx.doi.org/10.1021/acsaem.0c00926
ACS Appl. Energy Mater. 2020, 3, 7520−7526

agent compatible with the CZTS materials system could therefore be an approach to improve its properties.

4. CONCLUSIONS

By variation of annealing conditions, it was found that the device performance of CZTS thin-film solar cells as well as the materials properties of the CZTS absorber were highly dependent on the sulfur partial pressure. When insufficient sulfur was supplied or sulfur escaped the volume immediately surrounding the samples, the device performance significantly reduced. This was reflected in increased V_{oc} deficit and more extended band tails. A large variation in the amount of Cu−Zn disorder was observed in the samples. This could be related to the sulfur partial pressure during the annealing since insufficient sulfur causes a reduction in the vacancy concentration in CZTS and Sn loss in the near-surface region. While Cu−Zn disorder in itself is likely not the direct cause of the high V_{oc} deficit and tail state formation in CZTS, a low degree of ordering is indicative of a low vacancy concentration. A lower concentration of vacancies not only results in slower ordering dynamics but could also hinder efficient annihilation of other types of defects and grain growth due to reduced diffusion. Thus, we conclude that there is a need for better control of the anneal conditions, specifically to enhance diffusion and thereby improve crystal quality.

■ ASSOCIATED CONTENT

Supporting Information

The Supporting Information is available free of charge at https://pubs.acs.org/doi/10.1021/acsaem.0c00926.

Fitting of IQE measurements for determination of band tails, chemical composition after annealing, microstructure measured by cross-sectional SEM, X-ray diffraction correlated to voltage deficit, intensity-dependent photoluminescence, *JV* curves, device parameters, quantum efficiency, reflectance, Raman spectra, and photoluminescence spectra (PDF)

■ AUTHOR INFORMATION

Corresponding Author

J. K. Larsen − *Division of Solar Cell Technology, Department of Materials Science and Engineering, Uppsala University, Uppsala 752 36, Sweden;* orcid.org/0000-0002-7392-4701; Email: jes.larsen@angstrom.uu.se

Authors

J. J. S. Scragg − *Division of Solar Cell Technology, Department of Materials Science and Engineering, Uppsala University, Uppsala 752 36, Sweden;* orcid.org/0000-0001-8686-8721

N. Ross − *Division of Solar Cell Technology, Department of Materials Science and Engineering, Uppsala University, Uppsala 752 36, Sweden; Centre for Materials Science and Nanotechnology, University of Oslo, 0318 Oslo, Norway*

C. Platzer-Björkman − *Division of Solar Cell Technology, Department of Materials Science and Engineering, Uppsala University, Uppsala 752 36, Sweden;* orcid.org/0000-0002-6554-9673

Complete contact information is available at: https://pubs.acs.org/10.1021/acsaem.0c00926

Notes

The authors declare no competing financial interest.

■ ACKNOWLEDGMENTS

The authors acknowledge financial support from the Swedish Foundation for Strategic Research (grant no. RMA15-0030) and the Swedish Research Council (grant no. 2017-04336).

■ REFERENCES

(1) Yan, C.; Huang, J.; Sun, K.; Johnston, S.; Zhang, Y.; Sun, H.; Pu, A.; He, M.; Liu, F.; Eder, K.; Yang, L.; Cairney, J. M.; Ekins-Daukes, N. J.; Hameiri, Z.; Stride, J. A.; Chen, S.; Green, M. A.; Hao, X. Cu_2ZnSnS_4 Solar Cells with over 10% Power Conversion Efficiency Enabled by Heterojunction Heat Treatment. *Nat. Energy* **2018**, *3*, 764.

(2) Cui, X.; Sun, K.; Huang, J.; S. Yun, J.; Lee, C.-Y.; Yan, C.; Sun, H.; Zhang, Y.; Xue, C.; Eder, K.; Yang, L.; M. Cairney, J.; Seidel, J.; J. Ekins-Daukes, N.; Green, M.; Hoex, B.; Hao, X. Cd-Free Cu 2 ZnSnS 4 Solar Cell with an Efficiency Greater than 10% Enabled by Al 2 O 3 Passivation Layers. *Energy Environ. Sci.* **2019**, *12*, 2751−2764.

(3) Nakamura, M.; Yamaguch, K.; Kimoto, Y.; Yasaki, Y.; Kato, T.; Sugimoto, H. In *Cd-free Cu (In,Ga)(Se,S)2 Thin-film Solar Cell with a New World Recordefficacy of 23.35%*, 6th IEEE PVSC; IEEE: Chicago, IL, June 19, 2019.

(4) Rey, G.; Larramona, G.; Bourdais, S.; Choné, C.; Delatouche, B.; Jacob, A.; Dennler, G.; Siebentritt, S. On the Origin of Band-Tails in Kesterite. *Sol. Energy Mater. Sol. Cells* **2018**, *179*, 142−151.

(5) Gokmen, T.; Gunawan, O.; Todorov, T. K.; Mitzi, D. B. Band Tailing and Efficiency Limitation in Kesterite Solar Cells. *Appl. Phys. Lett.* **2013**, *103*, No. 103506.

(6) Scragg, J. J.; Larsen, J. K.; Kumar, M.; Persson, C.; Sendler, J.; Siebentritt, S.; Platzer Björkman, C. Cu−Zn Disorder and Band Gap Fluctuations in $Cu_2ZnSn(S,Se)_4$: Theoretical and Experimental Investigations. *Phys. Status Solidi (b)* **2016**, *253*, No. 189.

(7) Chen, S.; Walsh, A.; Gong, X.-G.; Wei, S.-H. Classification of Lattice Defects in the Kesterite Cu2ZnSnS4 and Cu2ZnSnSe4 Earth-Abundant Solar Cell Absorbers. *Adv. Mater.* **2013**, *25*, 1522−1539.

(8) Crovetto, A.; Hansen, O. What Is the Band Alignment of Cu2ZnSn(S,Se)4 Solar Cells? *Sol. Energy Mater. Sol. Cells* **2017**, *169*, 177−194.

(9) Siebentritt, S. Why Are Kesterite Solar Cells Not 20% Efficient? *Thin Solid Films* **2013**, *535*, 1−4.

(10) Chen, S.; Gong, X. G.; Walsh, A.; Wei, S.-H. Defect Physics of the Kesterite Thin-Film Solar Cell Absorber Cu2ZnSnS4. *Appl. Phys. Lett.* **2010**, *96*, No. 021902.

(11) Scragg, J. J. S.; Choubrac, L.; Lafond, A.; Ericson, T.; Platzer-Bjorkman, C. A Low-Temperature Order-Disorder Transition in Cu_2ZnSnS_4 Thin Films. *Appl. Phys. Lett.* **2014**, *104*, No. 041911.

(12) Rudisch, K.; Ren, Y.; Platzer-Björkman, C.; Scragg, J. Order-Disorder Transition in B-Type Cu2ZnSnS4 and Limitations of Ordering through Thermal Treatments. *Appl. Phys. Lett.* **2016**, *108*, No. 231902.

(13) Rey, G.; Redinger, A.; Sendler, J.; Weiss, T. P.; Thevenin, M.; Guennou, M.; El Adib, B.; Siebentritt, S. The Band Gap of $Cu_2ZnSnSe_4$: Effect of Order-Disorder. *Appl. Phys. Lett.* **2014**, *105*, No. 112106.

(14) Krämmer, C.; Huber, C.; Schnabel, T.; Zimmermann, C.; Lang, M.; Ahlswede, E.; Kalt, H.; Hetterich, M. In *Order-Disorder Related Band Gap Changes in Cu2ZnSn(S,Se)4: Impact on Solar Cell Performance*, 2015 IEEE 42nd Photovoltaic Specialist Conference (PVSC), 2015; pp 1−4.

(15) Davydova, A.; Rudisch, K.; Scragg, J. J. S. The Single Phase Region in Cu_2ZnSnS_4 Thin Films from Theory and Combinatorial Experiments. *Chem. Mater.* **2018**, *30*, 4624−4638.

(16) Rudisch, K.; Davydova, A.; Platzer-Björkman, C.; Scragg, J. The Effect of Stoichiometry on Cu-Zn Ordering Kinetics in Cu2ZnSnS4 Thin Films. *J. Appl. Phys.* **2018**, *123*, No. 161558.

(17) Valentini, M.; Malerba, C.; Menchini, F.; Tedeschi, D.; Polimeni, A.; Capizzi, M.; Mittiga, A. Effect of the Order-Disorder Transition on the Optical Properties of Cu2ZnSnS4. *Appl. Phys. Lett.* **2016**, *108*, No. 211909.

(18) Fedders, P. A.; Drabold, D. A.; Nakhmanson, S. Theoretical Study on the Nature of Band-Tail States in Amorphous Si. *Phys. Rev. B* **1998**, *58*, 15624−15631.
(19) Lang, M.; Renz, T.; Opolka, A.; Zimmermann, C.; Krämmer, C.; Neuwirth, M.; Kalt, H.; Hetterich, M. Impact of the Degree of Cu−Zn Order in $Cu_2ZnSn(S,Se)_4$ Solar Cell Absorbers on Defect States and Band Tails. *Appl. Phys. Lett.* **2018**, *113*, No. 033901.
(20) Bourdais, S.; Choné, C.; Delatouche, B.; Jacob, A.; Larramona, G.; Moisan, C.; Lafond, A.; Donatini, F.; Rey, G.; Siebentritt, S.; Walsh, A.; Dennler, G. Is the Cu/Zn Disorder the Main Culprit for the Voltage Deficit in Kesterite Solar Cells? *Adv. Energy Mater.* **2016**, *6*, No. 1502276.
(21) Gang, M. G.; Shin, S. W.; Suryawanshi, M. P.; Ghorpade, U. V.; Song, Z.; Jang, J. S.; Yun, J. H.; Cheong, H.; Yan, Y.; Kim, J. H. Band Tail Engineering in Kesterite $Cu_2ZnSn(S,Se)_4$ Thin-Film Solar Cells with 11.8% Efficiency. *J. Phys. Chem. Lett.* **2018**, *9*, 4555−4561.
(22) Moore, J. E.; Hages, C. J.; Agrawal, R.; Lundstrom, M. S.; Gray, J. L. The Importance of Band Tail Recombination on Current Collection and Open-Circuit Voltage in CZTSSe Solar Cells. *Appl. Phys. Lett.* **2016**, *109*, No. 021102.
(23) Scragg, J. J.; Ericson, T.; Kubart, T.; Edoff, M.; Platzer-Björkman, C. Chemical Insights into the Instability of Cu2ZnSnS4 Films during Annealing. *Chem. Mater.* **2011**, *23*, 4625−4633.
(24) Ren, Y.; Ross, N.; Larsen, J. K.; Rudisch, K.; Scragg, J. J.; Platzer-Björkman, C. Evolution of Cu_2ZnSnS_4 during Non-Equilibrium Annealing with Quasi-in Situ Monitoring of Sulfur Partial Pressure. *Chem. Mater.* **2017**, *29*, 3713−3722.
(25) Larsen, J. K.; Larsson, F.; Törndahl, T.; Saini, N.; Riekehr, L.; Ren, Y.; Biswal, A.; Hauschild, D.; Weinhardt, L.; Heske, C.; Platzer-Björkman, C. Cadmium Free Cu2ZnSnS4 Solar Cells with 9.7% Efficiency. *Adv. Energy Mater.* **2019**, *9*, No. 1900439.
(26) Lafond, A.; Choubrac, L.; Guillot-Deudon, C.; Deniard, P.; Jobic, S. Crystal Structures of Photovoltaic Chalcogenides, an Intricate Puzzle to Solve: The Cases of CIGSe and CZTS Materials. *Z. Anorg. Allg. Chem.* **2012**, *638*, 2571−2577.
(27) Larsen, J. K.; Keller, J.; Lundberg, O.; Jarmar, T.; Riekehr, L.; Scragg, J. J.; Platzer-Björkman, C. Sulfurization of Co-Evaporated $Cu(In,Ga)Se_2$ as a Postdeposition Treatment. *IEEE J. Photovoltaics* **2018**, *8*, 604−610.
(28) Larsen, J. K.; Li, S.-Y.; Scragg, J. J. S.; Ren, Y.; Hägglund, C.; Heinemann, M. D.; Kretzschmar, S.; Unold, T.; Platzer-Björkman, C. Interference Effects in Photoluminescence Spectra of Cu_2ZnSnS_4 and Cu $(In,Ga)Se_2$ Thin Films. *J. Appl. Phys.* **2015**, *118*, No. 035307.
(29) Lindahl, J.; Zimmermann, U.; Szaniawski, P.; Törndahl, T.; Hultqvist, A.; Salomé, P.; Platzer-Björkman, C.; Edoff, M. Inline $Cu(In,Ga)Se_2$Co-Evaporation for High-Efficiency Solar Cells and Modules. *IEEE J. Photovoltaics* **2013**, *3*, 1100−1105.
(30) Redinger, A.; Berg, D. M.; Dale, P. J.; Siebentritt, S. The Consequences of Kesterite Equilibria for Efficient Solar Cells. *J. Am. Chem. Soc.* **2011**, *133*, 3320−3323.
(31) Rühle, S. Tabulated Values of the Shockley−Queisser Limit for Single Junction Solar Cells. *Sol. Energy* **2016**, *130*, 139−147.
(32) Hages, C. J.; Carter, N. J.; Agrawal, R. Generalized Quantum Efficiency Analysis for Non-Ideal Solar Cells: Case of $Cu_2ZnSnSe_4$. *J. Appl. Phys.* **2016**, *119*, No. 014505.
(33) De Wolf, S.; Holovsky, J.; Moon, S.-J.; Löper, P.; Niesen, B.; Ledinsky, M.; Haug, F.-J.; Yum, J.-H.; Ballif, C. Organometallic Halide Perovskites: Sharp Optical Absorption Edge and Its Relation to Photovoltaic Performance. *J. Phys. Chem. Lett.* **2014**, *5*, 1035−1039.
(34) Miller, D. W.; Warren, C. W.; Gunawan, O.; Gokmen, T.; Mitzi, D. B.; Cohen, J. D. Electronically Active Defects in the Cu2ZnSn(Se,S)4 Alloys as Revealed by Transient Photocapacitance Spectroscopy. *Appl. Phys. Lett.* **2012**, *101*, No. 142106.
(35) Rey, G.; Weiss, T. P.; Sendler, J.; Finger, A.; Spindler, C.; Werner, F.; Melchiorre, M.; Hála, M.; Guennou, M.; Siebentritt, S. Ordering Kesterite Improves Solar Cells: A Low Temperature Post-Deposition Annealing Study. *Sol. Energy Mater. Sol. Cells* **2016**, *151*, 131−138.
(36) Levcenko, S.; Tezlevan, V. E.; Arushanov, E.; Schorr, S.; Unold, T. Free-to-Bound Recombination in near Stoichiometric Cu 2 ZnSnS 4 Single Crystals. *Phys. Rev. B* **2012**, *86*, No. 045206.
(37) Pan, Y. Monte Carlo Studies of Band-tail Effects on the Recombination Kinetics in Heavily Doped Silicon. *J. Appl. Phys.* **1990**, *67*, 7393−7398.
(38) Soldera, M.; Taretto, K.; Kirchartz, T. Comparison of Device Models for Organic Solar Cells: Band-to-Band vs. Tail States Recombination. *Phys. Status Solidi (a)* **2012**, *209*, 207−215.
(39) Dimitrievska, M.; Fairbrother, A.; Saucedo, E.; Pérez-Rodríguez, A.; Izquierdo-Roca, V. Influence of Compositionally Induced Defects on the Vibrational Properties of Device Grade Cu2ZnSnSe4 Absorbers for Kesterite Based Solar Cells. *Appl. Phys. Lett.* **2015**, *106*, No. 073903.
(40) Gouadec, G.; Colomban, P. Raman Spectroscopy of Nanomaterials: How Spectra Relate to Disorder, Particle Size and Mechanical Properties. *Prog. Cryst. Growth Charact. Mater.* **2007**, *53*, 1−56.
(41) Malerba, C.; Valentini, M.; Mittiga, A. Cation Disorder In Cu2ZnSnS4 Thin Films: Effect On Solar Cell Performances. *Solar RRL* **2017**, *1*, No. 1700101.
(42) Tuttle, J. R.; Contreras, M.; Bode, M. H.; Niles, D.; Albin, D. S.; Matson, R.; Gabor, A. M.; Tennant, A.; Duda, A.; Noufi, R. Structure, Chemistry, and Growth Mechanisms of Photovoltaic Quality Thin-film Cu(In,Ga)Se2 Grown from a Mixed-phase Precursor. *J. Appl. Phys.* **1995**, *77*, 153−161.
(43) McCandless, B. E.; Moulton, L. V.; Birkmire, R. W. Recrystallization and Sulfur Diffusion in CdCl2-Treated CdTe/CdS Thin Films. *Prog. Photovoltaics* **1997**, *5*, 249−260.

https://dx.doi.org/10.1021/acsaem.0c00926
ACS Appl. Energy Mater. 2020, 3, 7520−7526